Journal of Intelligent & Robotic Systems (2019) 94:327–338
https://doi.org/10.1007/s10846-018-0811-y

Robust Backstepping Control for a Four-Bar Linkage Mechanism Driven by a DC Motor

Mohammad Salah[1] · **Ahmad Al-Jarrah**[1] · **Enver Tatlicioglu**[2] · **Suleiman Banihani**[1]

Received: 15 August 2017 / Accepted: 7 March 2018 / Published online: 27 March 2018

Abstract

Four-bar linkage mechanisms have dragged the attention of many specialists due to its importance in the academic and industrial sectors. Hence, a lot of research work has been conducted to understand their complex behavior and explore various control techniques. In fact, such mechanisms possess highly nonlinear dynamics that require advanced nonlinear control methods. In addition, the four-bar linkage mechanism is exposed to significant dynamic fluctuations at high speeds due to the system inertias. In this paper, a backstepping control algorithm with a robust scheme is designed and applied on the four-bar linkage mechanism to investigate and explore its dynamical performance under various operating conditions and without a priori knowledge of the model parameters. Five operating conditions are introduced and tested in numerical simulations to show that the proposed nonlinear controller successfully regulates and tracks the speed of the driving link of the mechanism and shows a satisfactory performance.

Keywords Nonlinear system · Robust backstepping control · Four-bar mechanism · Mechatronics

Nomenclature List

B	vicious damping at motor bearing
C	torsional damping coefficient
cm_i	center of mass of the ith link
i_a	motor armature current
J	moment of inertia of the motor rotor and gear
J_i	moment of inertia of the ith link
K	torsional spring constant
k_b	motor electromotive force voltage constant
k_e	positive control gain
k_m	motor torque constant
k_o	positive control gain
k_η	positive control gain
L_a	motor armature inductance
L_i	length of inertia of the ith link
m_i	mass of inertia of the ith link
n	gear ratio
R_a	motor rotor armature resistor
r_i	location of the center of mass of the ith link
T	total applied torque on the leading link (i.e., link 2)
T_L	mechanical load torque
T_m	motor output torque
V_a	applied armature voltage
ε_1	arbitrary small positive constant
ε_2	arbitrary small positive constant
ε_i	arbitrary small positive constant
ε_x	arbitrary small positive constant
λ_1	positive constant
λ_2	positive constant
λ_3	positive constant
σ	small positive constant
$\ddot{\phi}_i$	angular acceleration of the ith link
$\dot{\phi}_i$	angular velocity of the ith link
ϕ_i	angular displacement of the ith link

✉ Mohammad Salah
msalah@hu.edu.jo

Ahmad Al-Jarrah
jarrah@hu.edu.jo

Enver Tatlicioglu
envertatlicioglu@iyte.edu.tr

Suleiman Banihani
banihani@hu.edu.jo

[1] Mechatronics Engineering Department, The Hashemite University, Zarqa 13115, Jordan

[2] Electrical and Electronics Engineering Department, Izmir Institute of Technology, Izmir, 35430, Turkey

1 Introduction

Four-bar linkage mechanisms are used in most moving machinery. Their simple mechanical design facilitates their use for path generation. For example, any change in the lengths of the bars or the driving angle will dramatically

affect the final output position, speed, and path. Moreover, the four-bar linkage mechanism is used in a variety of industrial applications such as rigid-body guidance, reciprocating compressor, rotary engine, scotch yoke, rope climbing robot, and robot end-effect gripper [10, 22, 29, 31]. Such mechanisms certainly are utilized to generate different motion patterns in comparison with actuators' motion [6, 9, 29]. In biomedical engineering, these mechanisms are employed to accomplish high-precision motion i.e., microsurgery applications) [4, 11, 14]. Many design difficulties could be created from such mechanisms; for example, the accuracy of the end-point positioning of a robot arm is considerably small because of the accumulated error from each revolute joint of the robot. In addition, having a poor mechanical stiffness will result in deterioration in the accuracy of the motion tracking [29, Zhang et al. 2005].

The mathematical model of the four-bar mechanism is well known. Nevertheless, it is assumed that the angular velocity of the driving bar (i.e., the crank) is constant. However, in practice this is almost impossible due to the fluctuating inertia of the rotary unbalanced mechanism. Hence, the angular speed of the crank in the four-bar mechanism shows a periodically changing behavior due to the continuous changes in inertia during the rotation of rigid links forming the mechanism [7, 9]. This fluctuating behavior results in a highly nonlinear, time-variant, and complex dynamics of the four-bar system which makes the control of such dynamics in real life a very complicated task and a challenge to design a control law that makes the four-bar mechanism follows a desired trajectory precisely at high speeds. Other techniques were proposed to model four-bar mechanisms such as [27, 28] where a parallelogram closed-loop mechanism was implemented into an open-loop robot structure to simplify the dynamics model of the overall system. High motion tracking performance was thus achieved by applying relatively simple control algorithms. Later, the author of [5] improved the motion tracking performance of the system by applying a mass redistribution scheme. In his study, the structure of a robotic arm was first reduced to dynamically equivalent point masses in order to eliminate the gravitational term in the dynamic model. A simple algorithm was then applied to control the system, and satisfactory trajectory tracking was obtained.

Other researchers focused on the synthesis of mechanisms for tracking trajectories; which is a well-known numerical optimization problem explored in depth in the literature. For instance, the authors of [8] introduced a computer programming-based design method of hybrid cam-linkage generating path using the theoretical contour equation of the cam. Moreover, the authors of [20] employed genetic algorithms for optimum synthesis of a four-bar linkage mechanism and the authors of [3] described the process of optimal synthesis of a four-bar linkage mechanism by the method of variable controlled deviations with the application of the differential evolution algorithm. On the other hand, [26] proposed an integrated mechanism and controller design approach to design variable input-speed servo four-bar linkages. The dimensions of the links, the counterweights, input speed trajectory, and controller parameters were considered as the design variables to reduce the shaking force and moment in order to improve the speed trajectory tracking performance, and to minimize the motor power dissipation. Finally, the authors of [24] presented a modified harmony search algorithm for the synthesis of a four-bar planar mechanism that follows a specific trajectory.

In fact, several operating methods, reported in the literature, are proposed to handle the complex nonlinear behavior of four-bar mechanisms such as [2, 30]. In [17], a proportional-derivative and neural adaptive superposed control was used to compensate for the global error. In [15], a control structure for the four-bar mechanism was introduced that was composed of several sub-control algorithms such as a model reference adaptive control, a disturbance compensation loop, and a modified switching controller, in addition to some feedback loops. In [14], an enhanced adaptive motion tracking control methodology without a feed-forward compensation was introduced for piezo-actuated flexure-based four-bar micro/nano manipulation mechanisms due to their nonlinear effect. Moreover, Erenturk [7] proposed a fuzzy logic controller combined with a gray system modeling approach to reduce the angular speed fluctuations in four-bar mechanisms driven by a permanent magnet dc motor that is fed from a dc–dc converter. Some other researchers such as [18] utilized intelligent methods to operate and control four-bar mechanisms due to the complexity of the dynamics. Recently, various control schemes were tested and applied, in simulation, for controlling the position and speed of a four-bar linkage mechanism [1] where the performance and response improvement were investigated thoroughly. In [1], a filtered proportional-integral-derivative controller (FPIDC) was tuned and implemented on the mechanism and then compared with a filtered sliding mode controller (FSMC), filtered fuzzy controller (FFC), and filtered genetic reinforcement neurocontroller (FGRNC). Moreover, in [23], the authors introduced a new intelligent model-free motion controller based on Fuzzy logic to improve robot motion accuracy and dynamic performance. They used a parametric search mechanism to identify system parameters with high accuracy. However, their method investigated a case with relatively low time-varying speed trajectory without any disturbances and/or parametric uncertainties. In addition, the proposed method requires either costly measuring devices or a complicated / inaccurate noisy calculation as a replacement for the costly measuring devices.

In this manuscript a robust backstepping controller is designed and tested, in simulation, to control the four-bar linkage mechanism and to investigate the performance under various operating conditions. It should be noted that the proposed controller has never been explored or introduced, in the literature, to operate such a mechanism. The proposed robust scheme is utilized to facilitate compensating for the uncertainties associated with the system dynamics. As for the backstepping scheme, it is a recursive Lyapunov-based scheme for strict feedback systems [12, 19, 25, 33]. Backstepping controller guarantees global or regional regulation and tracking criteria and provides a systematic procedure for designing stabilizing controllers, through a step by step algorithm. Moreover, it can avoid cancelations of useful nonlinearities and achieve stabilization and tracking [13]. Some other work introduced combinations of different control schemes such as [16]. In this manuscript, the implementation of a new control strategy is investigated and explored, in simulation, to further study new methods of control and their impact on the performance of a four-bar linkage mechanism under various operating conditions. The proposed control technique, in fact, does not require a priori knowledge of the model parameters and that is the key contribution and novelty of this work in addition to exploring new techniques of control on the introduced mechanism. In the future, real-time implementation shall be performed to validate the proposed control theory.

The sections introduced in the manuscript are organized as follows: Section 2 introduces the dynamics of the four-bar linkage mechanism. The proposed robust backstepping controller is introduced in Section 3 and representative numerical results are presented and discussed in Section 4. Finally, concluding remarks are presented in Section 5.

2 Dynamics of the Four Bar Linkage Mechanism

Figure 1 shows a schematic of the four-bar linkage mechanism introduced in this paper. As shown in Fig. 1, the first link of the mechanism, L_2, is driven by a geared permanent magnet dc motor. The complete mathematical model of the mechanism can be developed as reported in [1]

Referring to Fig. 1 and utilizing the torque equilibrium and the kinetic-potential equations with Lagrange's constraints along with Kirchoff's voltage law for the geared permanent magnet dc motor, the following mathematical expressions can be obtained [7]

$$\sum T = nT_m - nT_L - n^2 B\dot{\phi}_2 - n^2 J\ddot{\phi}_2 = A\ddot{\phi}_2 + \frac{1}{2}\frac{dA}{d\phi_2}\dot{\phi}_2^2 + K\gamma_4\left(\phi_4 - \phi_4(0)\right) + C\gamma_4^2\dot{\phi}_2 \quad (1)$$

$$V_a = L_a\frac{di_a}{dt} + i_a R_a + nk_b\dot{\phi}_2 \quad (2)$$

where the angular velocity of the i^{th} link can be computed by $\dot{\phi}_i = \gamma_i\dot{\phi}_2 \;\forall\; i = 2, 3, 4$, $\gamma_2 = 1$, $\gamma_3 = \frac{L_2\sin(\overline{\phi_4}-\phi_2)}{L_3\sin(\phi_3-\overline{\phi_4})}$, $\gamma_4 = \frac{L_2\sin(\phi_3-\phi_2)}{L_4\sin(\overline{\phi_4}-\phi_3)}$, and $\overline{\phi_4} = \phi_4 + \pi$ It should be noted that $L_3\sin\left(\dot{\phi}_3 - \dot{\phi}_4\right)$, $L_4\sin\left(\dot{\phi}_4 - \dot{\phi}_3\right)$, $L_3\sin^2\left(\dot{\phi}_3 - \dot{\phi}_4\right)$, and $L_4\sin^2\left(\dot{\phi}_3 - \dot{\phi}_4\right)$ do not equal to zero at any time. The function $A \in \mathbb{R}$ and its first derivative with respect to the angular displacement $\frac{dA}{d\phi_2} \in \mathbb{R}$, can be computed as

$$\frac{dA}{d\phi_2} \triangleq 2C_1\gamma_3\frac{d\gamma_3}{d\phi_2} + 2C_2\gamma_4\frac{d\gamma_4}{d\phi_2} + C_3\left\{\frac{d\gamma_3}{d\phi_2}\cos(\phi_3-\phi_2) - \gamma_3\sin(\phi_3-\phi_2)(\gamma_3-1)\right\} \quad (3)$$

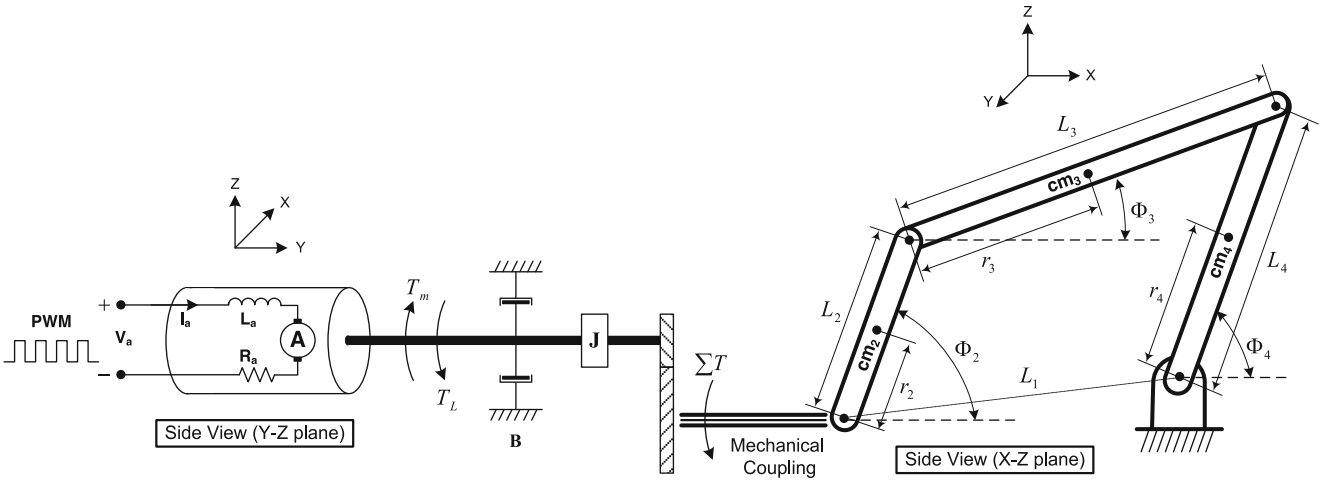

Fig. 1 A simplified schematic showing the complete four-bar linkage mechanism

where $A \triangleq C_0 + C_1\gamma_3^2 + C_2\gamma_4^2 + C_3\gamma_3\cos(\phi_3-\phi_2)$, $C_0 \triangleq J_2 + m_2r_2^2 + m_3L_2^2$, $C_1 \triangleq J_3 + m_3r_3^2$, $C_2 \triangleq J_4 + m_4r_4^2$, $C_3 \triangleq 2m_3r_3L_2$, $\frac{d\gamma_3}{d\phi_2} = \frac{L_2(D_1+D_2)}{L_3\sin^2(\phi_3-\phi_4)}$, $\frac{d\gamma_4}{d\phi_2} = \frac{L_2(D_3+D_4)}{L_4\sin^2(\phi_3-\phi_4)}$, $D_1 = (\gamma_4-1)\sin(\phi_3-\phi_4)\cos(\phi_4-\phi_2)$, $D_2 = (\gamma_4-\gamma_3)\sin(\phi_4-\phi_2)\cos(\phi_3-\phi_4)$, $D_3 = (\gamma_3-1)\sin(\phi_3-\phi_4)\cos(\phi_3-\phi_2)$, and $D_4 = (\gamma_4-\gamma_3)\sin(\phi_3-\phi_2)\cos(\phi_3-\phi_4)$ It should also be noted that the motor torque is defined as $T_m \triangleq k_m i_a$ and the parameters C and K in Eq. 1 are attached to the follower to represent a general loading situation. The entire mechanism is controlled by the applied armature voltage (i.e., motor input voltage / controller output), $V_a(t)$, which is affected indirectly by the armature current, $i_a(t)$. The armature current, in turns, controls the induced torque of the motor that operates the mechanism.

To facilitate the cont rol development, Eqs. 1 and 2 can be reformulated as follows

$$M\dot{x} + f_1 + g_1 = i_a \tag{4}$$

$$L_a\frac{di_a}{dt} + R_a i_a + Hx = V_a \tag{5}$$

where $x(t) \triangleq \dot{\phi}_2(t) \in \mathbb{R}$ is measurable, $H \triangleq nk_b \in \mathbb{R}^+$is a constant, and $M(x,t) \triangleq \frac{A+n^2J}{nk_m} \in \mathbb{R}$ is a positive definite function. It should be noted that the function $M(x,t)$ can be defined as a function of known and available quantities, Υ_m and an unknown/uncertain positive constants, Ψ_m, such that $M \triangleq M(\Upsilon_m, \Psi_m)$. The function $f_1(x,t) \in \mathbb{R}$ is defined as

$$f_1 \triangleq \frac{1}{2nk_m}\frac{dA}{d\phi_2}x^2 + \frac{C}{nk_m}\gamma_4^2 x + \frac{nB}{k_m}x + \frac{K}{nk_m}\gamma_4(\phi_4-\phi_4(0)) \tag{6}$$

and $g_1 \triangleq \frac{T_L}{k_m} \in \mathbb{R}^+$ is a constant and assumed to be always bounded. The function $f_1(x,t)$ can be considered as a function of known and available quantities denoted by $\Upsilon_1(t) \in \mathbb{R}^{1\times4}$ and unknown/uncertain positive constants denoted by $\Psi_1 \in \mathbb{R}^4$in the sense that $f_1 \triangleq f_1(\Upsilon_1, \Psi_1)$.

3 Robust Backstepping Controller Formulation

In this section, a robust backstepping control algorithm is introduced to regulate the output speed of the four-bar linkage mechanism and track desired speed trajectories if necessary under the presence of parametric uncertainties and disturbance for different operating conditions. The robustness feature is added to the controller to facilitate compensating for the uncertainties associated with the system dynamics. As a control objective, it is required to ensure that the angular velocity of the leading link, $x(t)$, tracks the desired trajectory $x_d(t) \in \mathbb{R}$, and the armature current, $i_a(t)$ tracks an auxiliary trajectory that represents the desired armature current, $i_{ad}(t) \in \mathbb{R}$, in the following sense

$$\{x_d(t)-x(t)\} \le \varepsilon_x \quad and \quad \{i_{ad}(t)-i_a(t)\} \le \varepsilon_i \quad as \quad t \to \infty \tag{7}$$

where $\varepsilon_x, \varepsilon_i \in \mathbb{R}^+$ are arbitrary small constants. It should be noted that the desired armature current is unknown *a priori* and will be designed later so that it is bounded at all times along with its first time derivative (i.e., $i_{ad}, \frac{di_{ad}}{dt} \in L_\infty$). Hence, the following error signal definitions are utilized to facilitate the controller design development

$$e \triangleq x_d - x \tag{8}$$

$$\eta \triangleq i_{ad} - i_a. \tag{9}$$

Based on the definitions in Eqs. 8 and 9, it is clear that if $|e(t)| \le \varepsilon_x$ and $|\eta(t)| \le \varepsilon_i$, then $|x_d(t)-x(t)| \le \varepsilon_x$ and $|i_{ad}(t)-i_a(t)| \le \varepsilon_i$ as $t \to \infty$, respectively, thus meeting the control objectives.

The open-loop error system dynamics can be analyzed by taking the first time derivative of Eqs. 8 and 9 and then multiplying both sides of the resulting equations by M and L_a, respectively. Thus, the system dynamics described in Eqs. 4 and 5 can be substituted and then reformatted to realize the following open-loop error system dynamics

$$M\dot{e} = M(\Upsilon_m, \Psi_m)\dot{x}_d + f_1(\Upsilon_1, \Psi_1) + g_1 + \eta - i_{ad} \tag{10}$$

$$L_a\dot{\eta} \triangleq L_a\frac{di_{ad}}{dt} + R_a i_a + Hx - V_a \tag{11}$$

where Eqs. 4, 5, 8, and 9 were utilized. The expression in Eq. 10, and after adding and subtracting $M(\Upsilon_{md}, \Psi_m) \in \mathbb{R}$ and $f_1(\Upsilon_{1d}, \Psi_1) \in \mathbb{R}$, can be further manipulated and rewritten as

$$M\dot{e} = \Lambda + \Pi + \eta - i_{ad} - \frac{1}{2}\dot{M}e \tag{12}$$

where the parameters $\Lambda, \Pi \in \mathbb{R}$ are defined as $\Lambda \triangleq M(\Upsilon_m, \Psi_m)\dot{x}_d - M(\Upsilon_{md}, \Psi_m)\dot{x}_d + f_1(\Upsilon_1, \Psi_1) - f_1(\Upsilon_{1d}, \Psi_1) + \frac{1}{2}\dot{M}e$ and $\Pi \triangleq M(\Upsilon_{md}, \Psi_m)\dot{x}_d + f_1(\Upsilon_{1d}, \Psi_1) + g_1$. It should be noted that $|\Lambda|$ can be upper bounded such that $|\Lambda| \le \rho_1(|e|)$ where $\rho_1(|e|) \in \mathbb{R}$ is a non-decreasing function of its argument. In addition, the terms Υ_{md} and $\Upsilon_{1d} \in \mathrm{R}^{1\times4}$are defined to be the desired forms of Υ_m and Υ_1, respectively.

Based on the open-loop error system dynamics introduced in Eq. 12, the following auxiliary control input (i.e., desired armature current) is designed

$$i_{ad} = \hat{\Pi} + k_e e + k_o\rho_1^2 e + v_{R_1} \tag{13}$$

where $\hat{\Pi} \triangleq M(\Upsilon_{md}, \hat{\Psi}_m)\dot{x}_d + f_1(\Upsilon_{1d}, \hat{\Psi}_1) + \hat{g}_1$ and $k_e, k_o \in \mathbb{R}^+$are control gain constants. The parameters $\hat{\Psi}_1 \in \mathbb{R}^4$ and

$\hat{g}_1 \in \mathbb{R}$ are constants and represent the best-guess estimates of Ψ_1 and g_1, respectively The parameter $v_{R_1}(\cdot) \in \mathbb{R}$ is a nonlinear robust term to compensate for the uncertain dynamics and shall be designed to ensure differentiability. Hence, the expression in Eq. 12, utilizing the auxiliary control input design, $i_{ad}(t)$, becomes

$$M\dot{e} = \Lambda + \tilde{\Pi} + \eta - k_e e - k_o \rho_1^2 e - \frac{1}{2}\dot{M}e - v_{R_1} \tag{14}$$

where $\tilde{\Pi} \triangleq \Pi - \hat{\Pi}$. Based on the design introduced in Eq. 13, the expression in Eq. 11 becomes

$$L_a \dot{\eta} \triangleq L_a \left\{ \dot{\hat{\Pi}} + k_e \dot{e} + 2k_o \rho_1 \frac{\partial \rho_1}{\partial e} e\dot{e} + k_o \rho_1^2 \dot{e} + \frac{\partial v_{R_1}}{\partial e}\dot{e} \right\} + R_a i_a + Hx - V_a \tag{15}$$

where $\dot{\hat{\Pi}} \triangleq \dot{M}(\Upsilon_{md}, \hat{\Psi}_m)\dot{x}_d + M(\Upsilon_{md}, \hat{\Psi}_m)\ddot{x}_d + \dot{f}_1(\Upsilon_{1d}, \hat{\Psi}_1)$. Note that $\dot{\hat{g}}_1 = 0$. The expression in Eq. 15 can be further manipulated and then reformulated to be

$$L_a \dot{\eta} \triangleq f_2 + g_2 - V_a \tag{16}$$

where the functions $f_2, g_2 \in \mathbb{R}$ are defined as

$$f_2 \triangleq L_a \left\{ \dot{\hat{\Pi}} + \left(k_e + 2k_o \rho_1 \frac{\partial \rho_1}{\partial e} e + k_o \rho_1^2 + \frac{\partial v_{R_1}}{\partial e} \right) M^{-1}(f_1 - i_a) \right\} + R_a i_a + Hx \tag{17}$$

$$g_2 \triangleq L_a \left(k_e + 2k_o \rho_1 \frac{\partial \rho_1}{\partial e} e + k_o \rho_1^2 + \frac{\partial v_{R_1}}{\partial e} \right) \left(\dot{x}_d + M^{-1} g_1 \right) \tag{18}$$

and Eqs. 4 and 8 were utilized. The function $f_2(x, t)$ can be considered as a function of known and available quantities denoted by $\Upsilon_2(t) \in \mathbb{R}^{1\times 8}$ and unknown/uncertain positive constants denoted by $\Psi_2 \in \mathbb{R}^{8\times 1}$ in the sense that $f_2 \triangleq f_2(\Upsilon_2, \Psi_2)$ Based on the open-loop error system dynamics introduced in Eqs. 16 to 18, the following controller is designed

$$V_a = k_\eta \eta + f_2\left(\Upsilon_{2d}, \hat{\Psi}_2\right) + e + v_{R_2} \tag{19}$$

where $k_\eta \in \mathbb{R}^+$ is a control gain constant, $\hat{\Psi}_2 \in \mathbb{R}^8$ is constant and represent the best-guess estimate of Ψ_2, and $\Upsilon_{2d} \in \mathbb{R}^{1\times 8}$is defined to be the desired form of Υ_2. The term $v_{R_2}(\cdot) \in \mathbb{R}$ is a nonlinear robust term to compensate for the uncertain dynamics and shall be designed to ensure differentiability. Hence, the expression in Eq. 16, utilizing the control input design, $V_a(t)$, becomes

$$L_a \dot{\eta} \triangleq f_2(\Upsilon_2, \Psi_2) - f_2(\Upsilon_{2d}, \Psi_2) + f_2(\Upsilon_{2d}, \Psi_2) - f_2\left(\Upsilon_{2d}, \hat{\Psi}_2\right) + g_2 - k_\eta \eta - e - v_{R_2} \tag{20}$$

where $f_2(\Upsilon_{2d}, \Psi_2)$ is added and subtracted to Eq. 16. In order to ensure the stability of the proposed control system, a Lyapunov-based stability analysis is introduced. Let $P(z, t) \in \mathbb{R}$ denote the following non-negative function

$$P \triangleq \tfrac{1}{2}Me^2 + \tfrac{1}{2}L_a \eta^2. \tag{21}$$

Note that Eq. 21 is bounded as (refer to Theorem 2.14 of [21])

$$\lambda_1 \|z(t)\|^2 \leq P(z, t) \leq \lambda_2 \|z(t)\|^2 \tag{22}$$

where $\lambda_1, \lambda_2 \in \mathbb{R}^+$ are constants and $z\left[e, \eta\right]^T \in \mathbb{R}^2$ where $e(t)$ and $\eta(t)$ are defined in Eqs. 10 and 11, respectively. After taking the first time derivative of the expression in Eq. 21, then

$$\dot{P} \triangleq e\left\{\Lambda + \tilde{\Pi} + \eta - k_e e - k_o \rho_1^2 e - v_{R_1}\right\} + \eta\left\{f_2(\Upsilon_2, \Psi_2) - f_2(\Upsilon_{2d}, \Psi_2) + f_2(\Upsilon_{2d}, \Psi_2) - f_2\left(\Upsilon_{2d}, \hat{\Psi}_2\right) + g_2 - k_\eta \eta - e - v_{R_2}\right\} \tag{23}$$

where Eqs. 14 and 20 were utilized. Based on the expression developed in Eq. 23, the nonlinear robust functions, $v_{R_1}(t)$ and $v_{R_2}(t)$ can be designed as

$$v_{R_1} = \frac{e\rho_{2,s}^2}{\|e\|_m \rho_{2,m} + \varepsilon_1} \tag{24}$$

$$v_{R_2} = \frac{\eta\rho_3^2}{|\eta|\rho_3 + \varepsilon_2} \tag{25}$$

Table 1 Simulated cases introduced to investigate controller performance

Case	Desired Tracking Trajectory [rpm]	Disturbance [N.m]
I	$n_d = 100$	$T_L = 1$
II	$n_d = 100$	$T_L = 1.3 - 0.025\,cos\,(30\pi t) - 0.05\,cos\,(20\pi t) - 0.05\,cos\,(10\pi t) - 0.125\,cos\,(16\pi t)$
III	$n_d = 10\,sin\,(4\pi t) + 100$	$T_L = 1$
IV	$n_d = 10\,sin\,(4\pi t) + 100$	$T_L = 1.3 - 0.025\,cos\,(30\pi t) - 0.05\,cos\,(20\pi t) - 0.05\,cos\,(10\pi t) - 0.125\,cos\,(16\pi t)$
V	$n_d = 10\,sin\,(4\pi t) + 100$	$T_L = 1.3 - 0.025\,cos\,(30\pi t) - 0.05\,cos\,(20\pi t) - 0.05\,cos\,(10\pi t) - 0.125\,cos\,(16\pi t)$ and parametric uncertainties

Table 2 Simulation parameter values for the introduced four-bar linkage mechanism

Parameter	Value	Unit	Parameter	Value	Unit	Parameter	Value	Unit
B	0.2	N.s/m	K	5	N/m	n	0.95	–
C	5	N.s/m	L_2	0.1349	m	$\phi_2\,(0)$	1.5708	Rad
J	0.011	kg.m^2	L_3	0.2997	m	$\phi_3\,(0)$	0.5196	Rad
J_2	0.000269	kg.m^2	L_4	0.3251	m	$\phi_4\,(0)$	1.6443	Rad
J_3	0.00219	kg.m^2	L_a	0.014	H	r_2	0.0674	m
J_4	0.00229	kg.m^2	m_2	0.09919	kg	r_3	0.1488	m
k_b	0.26	V.s/rad	m_3	0.1794	kg	r_4	0.1625	m
k_m	0.26	–	m_4	0.1765	kg	R_a	2	Ω

where $\varepsilon_1, \varepsilon_2 \in \mathbb{R}^+$ are small constants, $\rho_{2,s}, \rho_{2,m} \in \mathbb{R}$ are defined as $\rho_{2,s} \triangleq \rho_2\left(\|e\|_s\right)$ and $\rho_{2,m} \triangleq \rho_2\left(\|e\|_m\right)$ where $\|e\|_s \triangleq \sqrt{e^2+\sigma}$, $\|e\|_m \triangleq \sqrt{e^2+\sigma} - \sqrt{\sigma}$, and $\sigma \in \mathbb{R}^+$ is a small constant. It should be noted that $\tilde{\Pi} \leq \rho_2\left(|e|\right)$ where $|e|$ is bounded as $\|e\|_s \geq |e| \geq \|e\|_m$. The function $\rho_3\left(|e|\right) \in \mathbb{R}$ is a non-decreasing function of its argument. Moreover, the following inequalities are satisfied

$$e\,\Lambda - k_o \rho_1^2 e^2 \leq |e|\,\rho_1 - k_o \rho_1^2 e^2 \leq \frac{1}{4k_o} \tag{26}$$

$$e\,\tilde{\Pi} \leq |e|\;\rho_2 \tag{27}$$

$$\eta \left\{ f_2\left(\Upsilon_2, \Psi_2\right) - f_2\left(\Upsilon_{2d}, \Psi_2\right) + f_2\left(\Upsilon_{2d}, \Psi_2\right) - f_2\left(\Upsilon_{2d}, \hat{\Psi}_2\right) + g_2 \right\} \leq |\eta|\left(c_1\,|\eta| + c_2\right) \leq |\eta|\,\rho_3 \tag{28}$$

where $c_1, c_2 \in \mathbb{R}^+$ are constants. Based on the inequalities introduced in Eqs. 26 to 28, the expression in Eq. 23 can be upper bounded by

$$\dot{P} \leq -k_e e^2 - k_\eta \eta^2 + \frac{1}{4k_o} + |e|\;\rho_2 - e\,v_{R_1} + |\eta|\,\rho_3 - \eta\;v_{R_2}. \tag{29}$$

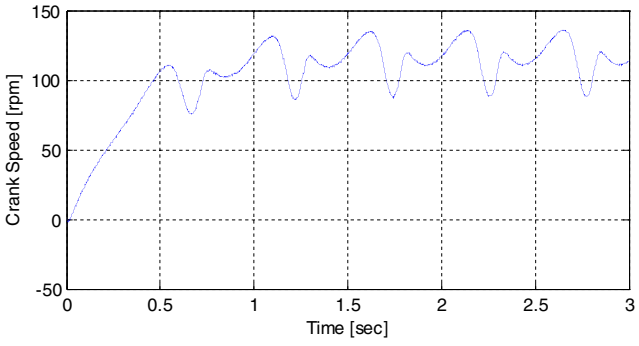

Fig. 2 Crank speed open-loop response when 12V input voltage is applied

Note that the following inequalities are satisfied based on the design introduced in Eqs. 24 and 25

$$|e|\;\rho_2 - e\,v_{R_1} = |e|\;\rho_2 - \frac{e^2\rho_{2,s}^2}{\|e\|_m\,\rho_{2,m} + \varepsilon_1} \leq \varepsilon_1 \tag{30}$$

$$|\eta|\,\rho_3 - \eta\;v_{R_2} = |\eta|\,\rho_3 - \frac{\eta^2\rho_3^2}{|\eta|\,\rho_3 + \varepsilon_2} \leq \varepsilon_2 \tag{31}$$

Hence, the function $\dot{P}(z,t) \in \mathbb{R}$ obtained in Eq. 29 can be upper bounded as

$$\dot{P} \leq -\lambda_3\,\|z\|^2 + \varepsilon \tag{32}$$

where $\lambda_3 \geq k_e + k_\eta$ and $\varepsilon \triangleq \frac{1}{4k_o} + \varepsilon_1 + \varepsilon_2$ and that satisfies the globally ultimately bounded stability result.

4 Numerical Simulations

In this section, numerical results are presented in Matlab/Simulink environment to demonstrate the effectiveness and feasibility of using the proposed robust backstepping controller, introduced in Eqs. 13, 19, 24, and 25, in regulating and tracking a prescribed speed trajectory. It should be noted that the capabilities of the modern hardware and relatively slow dynamics of introduced mechanical system allow the detailed controller design to be implemented without concerns in the laboratory. Five cases are examined by

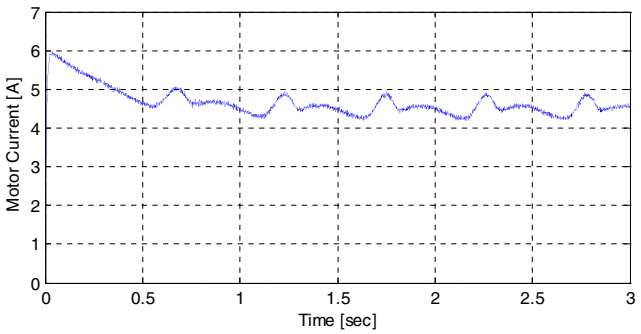

Fig. 3 Motor current response when 12V input voltage is applied

Table 3 Tuned gains for the proposed controller

Parameter	Value	Parameter	Value
ε_1	0.01	ρ_1	$100\,\lvert e\rvert$
ε_1	0.01	$\rho_{2,m}$	$\lVert e\rVert_m$
k_e	100	$\rho_{2,s}$	$100\,\lVert e\rVert_s$
k_η	100	ρ_3	$100\,\lvert e\rvert$
ko	0.1	σ	0.1

the proposed controller in this section: (i) constant desired speed trajectory with constant load torque disturbance, (ii) constant desired speed trajectory with time-varying load torque disturbance (iii) time-varying desired speed trajectory with constant load torque disturbance, (iv) time-varying desired speed trajectory with time-varying load torque disturbance, and (v) time-varying desired speed trajectory with time-varying load torque disturbance and parametric uncertainties. More details about the proposed cases are shown in Table 1.

It should be noted that cases II and IV are introduced to more challenge the controller. However, Case V is the most challenging case among all cases. In Case V, the system parameters are set to vary with respect to time around their original values by 5% for some parameters and 10% for the others at different frequencies such that: $L_a = 0.0007\sin(20\pi t) + 0.014$, $R_a = 0.1\cos(24\pi t) + 2$, $k_b = 0.013\sin(30\pi t) + 0.26$, $k_m = 0.013\cos(30\pi t) + 0.26$, $J = 0.00055\cos(20\pi t) + 0.011$, $J_2 = 0.0000269\sin(20\pi t) + 0.000269$, $J_3 = 0.000219\cos(24\pi t) + 0.00219$, $J_4 = 0.000229\sin(30\pi t) + 0.00229$, $L_2 = 0.01349\sin(20\pi t) + 0.1349$, $L_3 = 0.02997\cos(24\pi t) + 0.2997$, $L_4 = 0.03251\sin(30\pi t) + 0.3251$, $m_2 = 0.09919\sin(20\pi t) + 0.9919$, $m_3 = 0.01794\cos(24\pi t) + 0.1794$, $m_4 = 0.01765\sin(30\pi t) + 0.1765$, $r_2 = 0.00674\sin(20\pi t) + 0.0674$, $r_3 = 0.01488\cos(24\pi t) + 0.1488$, $r_4 = 0.01625\sin(30\pi t) + 0.1625$, $C = 0.5\cos(20\pi t) + 5$, $K = 0.5\sin(20\pi t) + 5$. Despite of the unrealistic parametric conditions presented in Case V, it is introduced to mainly investigate the controller performance under the presence of parametric uncertainties.

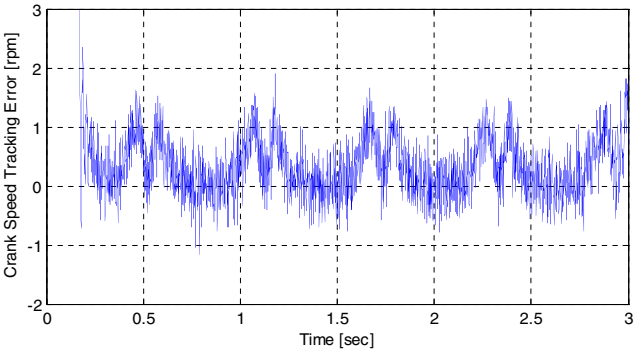

Fig. 5 Speed tracking error for Case I

In order to have more realistic performance for all introduced simulated tests, a band limited white noise of power 1μ and sampling time of 100μsec is added to all measurements. In addition, the motor rated voltage is limited to ±24V. The simulation was implemented with Bogacki-Shampine (ode3) solver and 100μsec sampling time. Table 2 shows all parameter values for the proposed four-bar linkage mechanism. For the sake of comparison, the open-loop response of the crank angular velocity is shown in Fig. 2 for a step input voltage of 12V (that is applied to the mechanism driving motor). As shown in Fig. 2, the speed fluctuates due to the system inertia variations during rotation. The fluctuations are observed to be between 87.5 and 135.5 rpm. Figure 3 shows the current withdrawn by the DC motor under open-loop condition which matches the variations in the system inertia during rotation.

In all introduced cases, a low-pass filter, that is tuned at $\left(\frac{0.01}{100s+1}\right)$, is implemented on the controlled input voltage to smoothen the chattering that could occur. Moreover, the proposed controller gains are tuned to achieve a satisfactory performance as listed in Table 3. For Case I, Figs. 4, 5, 6, and 7 show the crank speed response of the closed-loop system, speed tracking error, control input voltage,

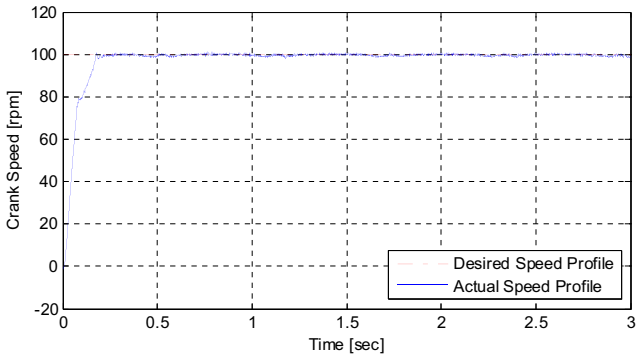

Fig. 4 Crank speed response for Case I

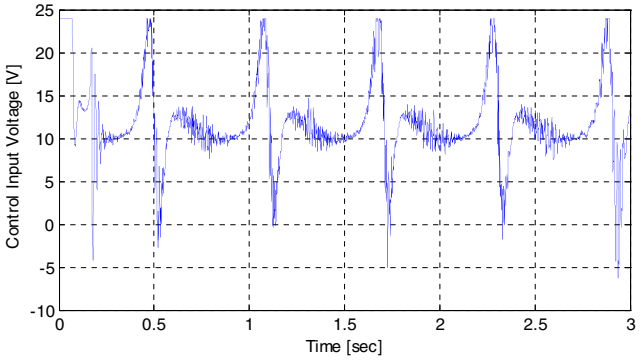

Fig. 6 Control input voltage for Case I

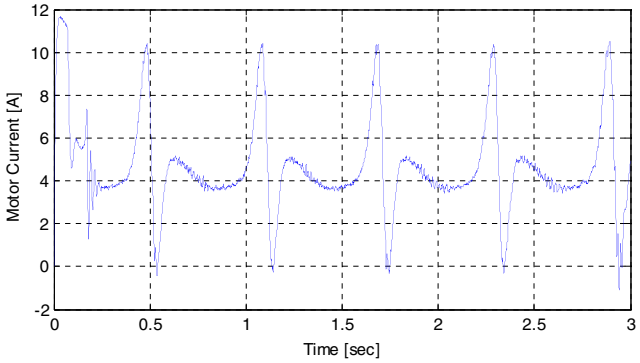

Fig. 7 Motor Current for Case I

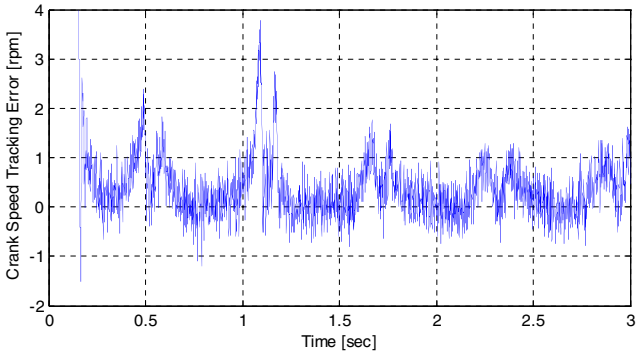

Fig. 9 Speed tracking error for Case III

and motor current, respectively. As shown in Figs. 4 and 5, the response is fast and smooth and speed tracking error does not exceed 1.5 rpm (i.e., 1.5% of final value) at steady state. The control input voltage and motor current change accordingly to keep the crank speed track the desired trajectory accordingly as shown in Figs. 6 and 7.

Figures 8, 9, 10, and 11 show the crank speed response of the closed-loop system, speed tracking error, control input voltage, and motor current, respectively, for Case III. This case is introduced to investigate the response of the controller in case the desired speed trajectory varies with respect to time and set to a relatively high frequency (i.e., 2 Hz). As shown in Fig. 8, the response is fast and smooth. Although the desired speed trajectory varies with time within ±5 rpm, the speed tracking error does not exceed 1.5 rpm (i.e., 1.5% of final value) at steady state as shown in Fig. 9. For this speed trajectory, more effort is required as shown in Fig. 10 when the control input voltage hits the maximum at 24 V and chatters a lot afterward. The motor current variations are relatively smooth and acceptable as shown in Fig. 11.

To more challenge the proposed controller, a load torque disturbance is introduced for cases II and IV as shown in Fig. 12. Figures 13 and 14 show the crank speed response of the closed-loop system and speed tracking error, respectively, for Case II. As shown in Fig. 13, the speed tracking is very acceptable and satisfactory. The speed tracking error does not exceed, in this case, 1.5 rpm (i.e., 1.5% of final value) at steady state as shown in Fig. 14. For this applied load torque disturbance, more effort is required in comparison to Case I. More chattering can be observed in the control input voltage and motor current as shown in Figs. 15 and 16. When Case IV is simulated and tested, the proposed controller is significantly challenged. Nevertheless, the controller performs satisfactorily and tracks the desired speed trajectory successfully with a maximum tracking error of 2 rpm (i.e., 2% of final value) at steady state as shown in Figs. 17 and 18. However, about 7.5 rpm overshoot is observed but occurs within the first 0.2 sec of operation. The control input voltage and motor current are shown in Figs. 19 and 20. As shown from the figures, the response is acceptable in order to achieve a satisfactory speed tracking under the introduced conditions.

It should be noted that in all cases, the motor rated voltage is not allowed to exceed ±24V and that explains why the speed regulation or tracking is not precise at certain times as shown in Figs. 4, 8, 13, and 17. The associated saturated applied motor voltages are shown in Figs. 6, 10, 15, and 19. In order to present a quantitative comparison between the four cases, two measures are introduced and computed to quantify the performance of the proposed controller under the conditions listed in Table 1:

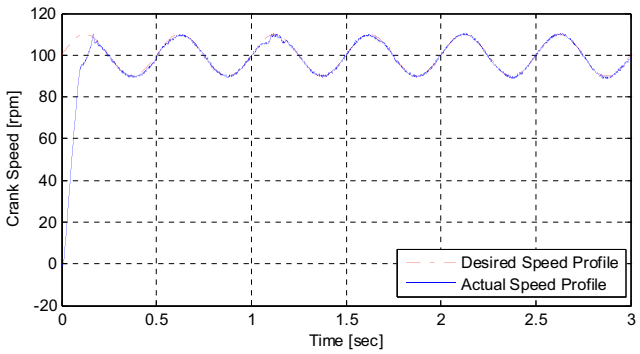

Fig. 8 Crank speed response for Case III

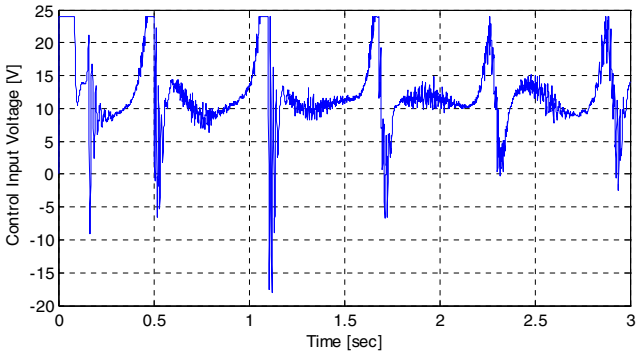

Fig. 10 Control input voltage for Case III

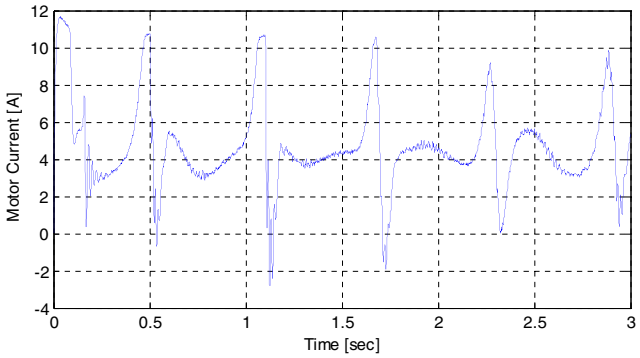

Fig. 11 Motor current for Case III

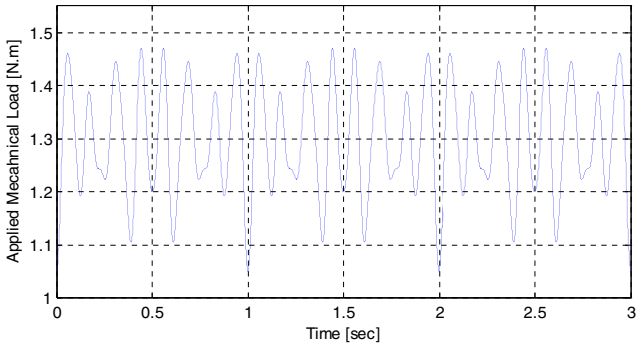

Fig. 12 Applied mechanical load for cases II and IV

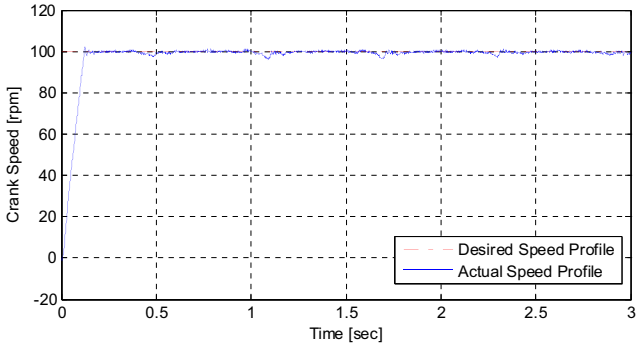

Fig. 13 Crank speed response for Case II

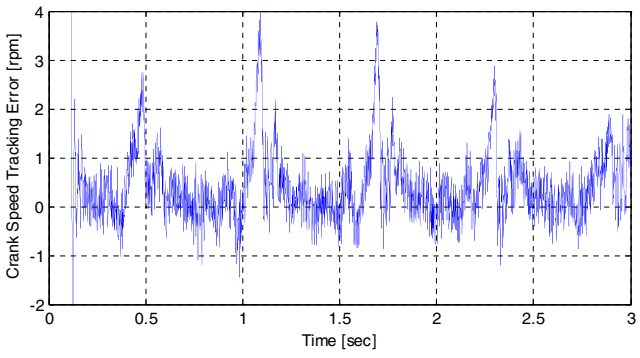

Fig. 14 Speed tracking error for Case II

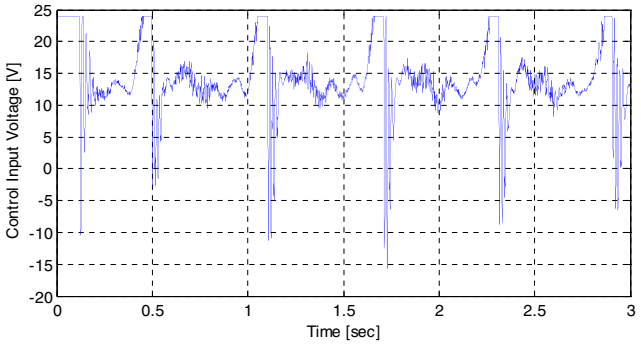

Fig. 15 Control input voltage for Case II

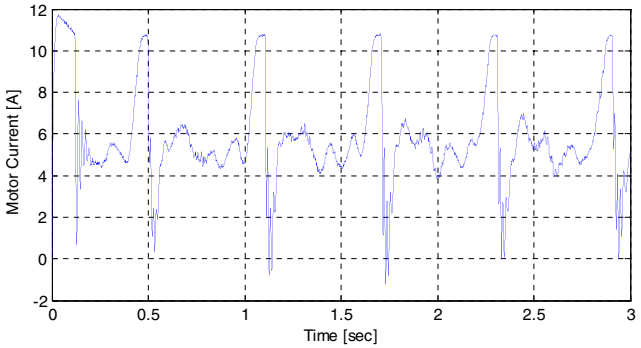

Fig. 16 Motor current for Case II

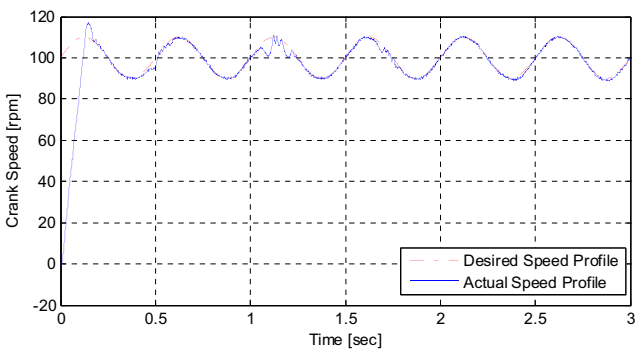

Fig. 17 Crack speed response for Case IV

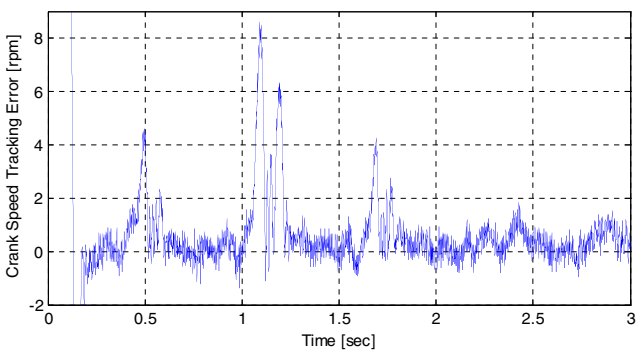

Fig. 18 Speed tracking error for Case IV

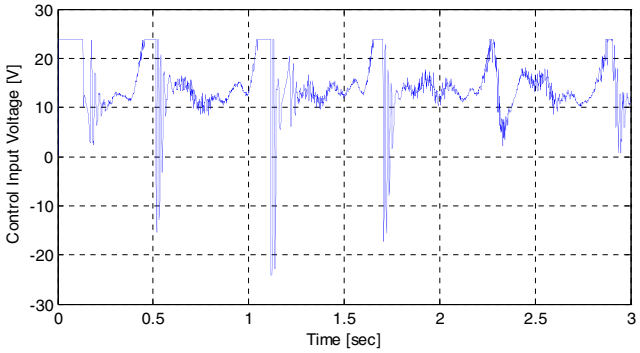

Fig. 19 Control input voltage for Case IV

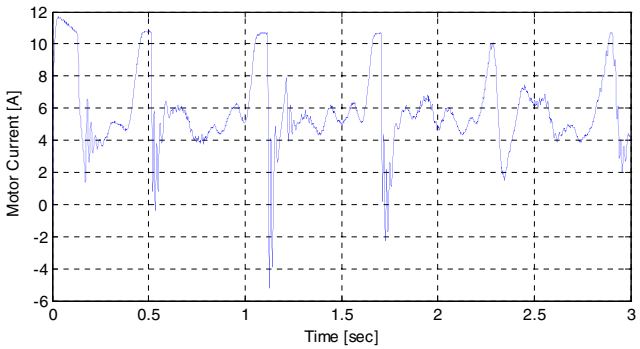

Fig. 20 Motor current for Case IV

Table 4 Controller effort and speed tracking error measures along with steady-state absolute error for cases I, II, III, and IV

Case	M_u	M_e	|e|
I	487.4	408	1.5
II	502.3	442.3	1.5
III	690.8	445.8	1.5
IV	700	512.6	2

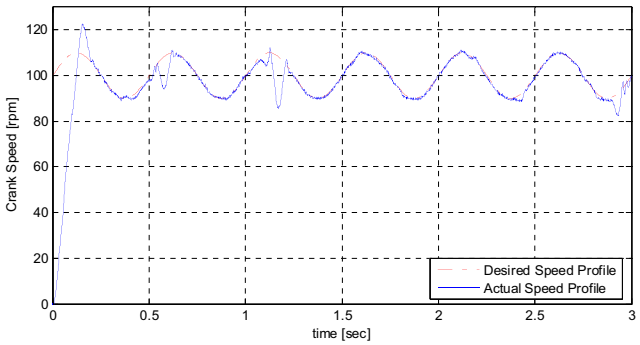

Fig. 21 Crack speed response for Case V

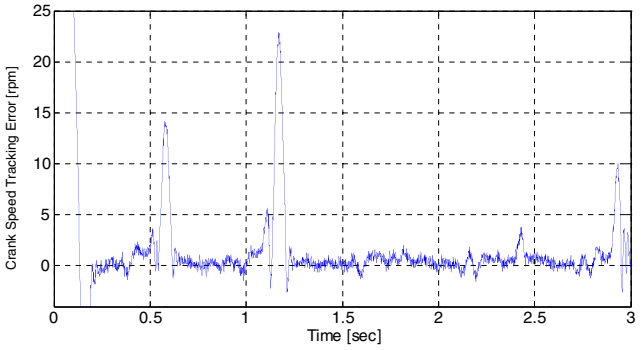

Fig. 22 Speed tracking error for Case V

(1) $M_u = \int_0^T |V_a(\tau)|^2 d\tau$, and (2) $M_e = \int_0^T |e(\tau)|^2 d\tau$

where the measures M_u and M_e are for the energy expanded by the controller and for the speed tracking error over the period of system operation (i.e., T = 3 sec), respectively. The introduced quantities for cases I, II, III, and IV are shown in Table 4 As shown from the table, speed tracking error is better when tracking a constant speed in comparison with a time-varying speed. In addition, controller effort is less in Case I in comparison with Case III. Moreover, in cases II and IV, more effort is required by the controller in comparison with cases I and III where the load torque disturbance is constant. In Table 4, and for the sake of comprehensive comparison, the steady-state absolute tracking error is recorded.

Finally, Case V is introduced to even more challenge the proposed controller in comparison with cases II and IV. This case is the most challenging case introduced to test the robustness and validity of the proposed controller. In this case, time-varying desired speed trajectory with time-varying load torque disturbance and parametric uncertainties are introduced. In fact, this case may not be logical in reality but introduces a very solid case to test the system parametric uncertainties. Figures 21 and 22 show the crank speed response of the closed-loop system and speed tracking error, respectively, for Case V. As shown in Fig. 21, the speed

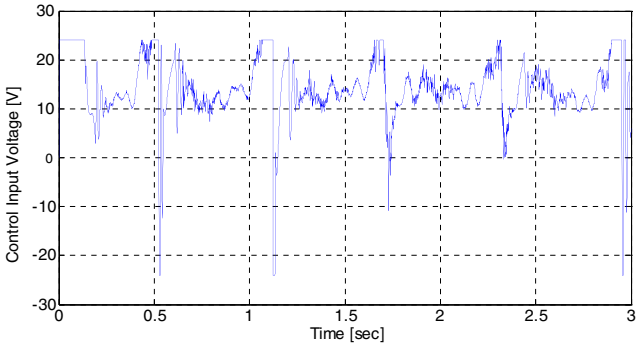

Fig. 23 Control input voltage for Case V

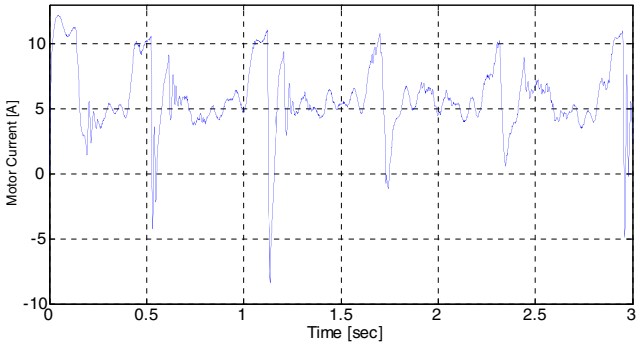

Fig. 24 Motor current for Case V

tracking is very acceptable and satisfactory at the times where the motor voltage is not saturated (i.e., more effort by the motor is not allowed to get the mechanism speed into track). This is clear in Fig. 23. The motor current associated with the fluctuations of the motor voltage is shown in Fig. 24. The steep behavior of the motor current is clear due to the sudden demand of motor torque to correct the speed track that is limited by the motor voltage saturation. Overall, the proposed controller shows a satisfactory performance under the presence of parametric uncertainties.

5 Concluding Remarks

In this paper, a robust backstepping controller is designed and tested, in simulation, for a four-bar linkage mechanism that is driven by a dc motor. An advanced controller such as the proposed one has never been applied on such mechanism that is considered to be an important part of many applications in the academic and industrial sectors. It has been a challenge to design a nonlinear controller such as the proposed one to tackle the complex behavior associated with the four-bar linkage mechanism nonlinear dynamics. From the introduced simulation results it is clear that the proposed robust backstepping nonlinear controller is capable of regulating the speed and tracking a desired speed trajectory of the four-bar linkage mechanism satisfactorily, under different operating conditions, despite of the significant dynamic fluctuations observed in the open-loop system dynamics. It should also be noted that the proposed robust controller was designed so that a priori knowledge of the model parameters is not required. Finally, the feasibility of using such nonlinear controller on the four-bar linkage mechanism was proven. Experimental testing will be considered as a future work.

Acknowledgments Work of E. Tatlicioglu is partially supported by The Scientific and Technological Research Council of Turkey via grant number 116M272.

References

1. Al-Jarrah, A., Salah, M., Banihani, S., Al-Widyan, K., Ahmad, A.: Applications of various control schemes on a Four–Bar linkage mechanism driven by a geared DC motor. WSEAS Trans. Syst. Control **10**, 584–597 (2015)
2. Boscariol, P., Gasparetto, A., Zanotto, V.: Model predictive control of a flexible links mechanism. J. Intell. Robot. Syst. **58**(2), 125–147 (2010)
3. Bulatovic, R., Dordevic, S.: On the optimum synthesis of a four-bar linkage using differential evolution and method of variable controlled deviations. Mech. Mach. Theory **44**(1), 235–246 (2009)
4. Choudhary, V.B., Singh, V.K., Dutta, A.: Design of an optimal 4-bar mechanism based gravity balanced leg orthosis. J. Intell. Robot. Syst. **86**(3-4), 485–494 (2017)
5. Diken, H.: Trajectory control of mass balanced manipulator. Mech. Mach. Theory **32**(3), 313–322 (1997)
6. Ebrahimi, S., Payvandy, P.: Efficient constrained synthesis of path generating four bar mechanisms based on the heuristic optimization algorithms. Mech. Mach. Theory **85**, 189–204 (2015)
7. Erentürk, K.: Hybrid control of a mechatronic system: fuzzy logic and grey system modeling approach. IEEE/ASME Trans. Mechatronics **12**(6), 703–710 (2007)
8. Ge, Z., Li, X., Ren, Z., Yang, F.: Research on the Hybrid Cam-Linkage Mechanism Realizing Trajectory. In: International Technology and Innovation Conference (ITIC), Hangzhou, China, pp. 2012–2016 (2006)
9. Gündoğdu, Ö., Erentürk, K.: Fuzzy control of a dc motor driven four-bar mechanism. Mechatronics **15**(4), 423–438 (2005)
10. Hassan, A., Abomoharam, M.: Design of a Single DOF Gripper Based on Four-Bar and Slider-Crank Mechanism for Educational Purposes. In: 24th CIRP Design Conference, Procedia CIRP, vol. 21, pp. 379–384 (2014)
11. Huang, T.-H., Huang, H.-P., Kuan, J.-Y.: Mechanism and control of Continuous-State coupled elastic actuation. J. Intell. Robot. Syst. **74**(3-4), 571–587 (2014)
12. Khalil, H.: Nonlinear Systems. 3rd Ed. Prentice Hall (2002)
13. Krstic, M., Kanellakopoulos, I., Kokotovic, P.: Nonlinear and Adaptive Control Design. Wiley, New York (1995)
14. Liaw, H.-C., Shirinzadeh, B.: Enhanced adaptive motion tracking control of piezoactuated flexure-based four-bar mechanisms for micro/nano manipulation. Sensors Actuators A Phys. **147**(1), 254–262 (2008)
15. Lin, M.-C., Chen, J.-S.: Experiments toward MRAC design for linkage system. Mechatronics **6**(8), 933–953 (1996)
16. Liu, Y.-H.: Saturated robust adaptive control for uncertain nonlinear systems using a new approximate model. IET Control Theory Appl. **11**(6), 870–876 (2017)
17. Lungu, R., Sepcu, L., Lungu, M.: Four-bar mechanism's proportional-derivative and neural adaptive control for the thorax of the micromechanical flying insects. ASME J Dyn. Syst., Measurement, and Control **137**(5), 051005–0510017 (2015)
18. Maeda, Y., De Figueiredo, R.J.B.: Learning rules for neuro-controller via simultaneous perturbation. IEEE Trans. Neural Netw. **8**(5), 1119–1130 (1997)
19. Marquez, H.: Nonlinear Control Systems – Analysis and Design. Wiley, New York (2003)
20. Nariman-Zadeh, N., Felezi, M., Jamali, A., Ganji, M.: Pareto optimal synthesis of four-bar mechanisms for path generation. Mech. Mach. Theory **44**(1), 180–191 (2009)
21. Qu, Z.: Robust Control of Nonlinear Uncertain Systems. Wiley, New York (1998)
22. Rajesh Kanna, G., Ashik, M.: Design and development of a rope climbing robot using four bar mechanism with wireless control using TX2/RX2 RF Module. In: IEEE International Conference

on Signal Processing, Informatics, Communication and Energy Systems (SPICES), Kozhikode, India, pp. 1–6 (2015)
23. Ren, Q., Bigras, P.: A highly accurate model-free motion control system with a Mamdani fuzzy feedback controller Combined with a TSK fuzzy feed-forward controller. J. Intell. Robot. Syst. **86**(3–4), 367–379 (2017)
24. Sánchez-Márquez, Á., Vega-Alvarado, E., Alfredo Portilla-Flores, E., Mezura-Montes, E.: Synthesis of a Planar Four-Bar Mechanism for Position Control Using the Harmony Search Algorithm. In: 11Th International Conference on Electrical Engineering, Computing Science, and Automatic Control (CCE), Campeche, Mexico, pp. 1–6 (2014)
25. Ting, C.-S., Chang, Y.-N., Shi, B.-W., Lieu, J.-F.: Adaptive backstepping control for permanent magnet linear synchronous motor servo drive. IET Electr. Power Appl. **9**(3), 265–279 (2015)
26. Yan, H.-S., Yan, G.-J.: Integrated control and mechanism design for the variable input-speed servo four-bar linkages. Mehcatronics **19**(2), 274–285 (2009)
27. Youcef-Toumi, K.: Analysis, Design and Control of Direct Drive Manipulators PhD Dissertation. Mechanical Engineering Department, Massachusetts Institute of Technology (1985)
28. Youcef-Toumi, K., Kuo, A.: High-speed trajectory control of a direct-drive manipulator. IEEE Trans. Robot. Autom. **9**(1), 102–108 (1993)
29. Zhang, W., Chen, X.: Mechatronics design for a programmable closed-loop mechanism. Proc. IME C J Mech. Eng. Sci. **215**(3), 365–375 (2001)
30. Zhang, K.: Research on high precision control system of a hybrid five-bar actuator. In: International Technology and Innovation Conference (ITIC), Hangzhou, China, pp. 2149–2154 (2006)
31. Zhang, W.J., Li, Q., Guo, L.S.: Integrated design of mechanical structure and control algorithm for a programmable four-bar linkage. IEEE/ASME Trans. Mechatron. **4**(4), 354–362 (1999)
32. Zhang, Z., Park, J.H., Shao, H., Qi, Z.: Exact tracking control of uncertain non-linear systems with additive disturbance. IET Control Theory Appl. **9**(5), 736–744 (2015)
33. Zhao, H.: Application of robust adaptive backstepping control in a class of uncertain nonlinear system. In: International Conference on Automatic Control and Artificial Intelligence (ACAI), Xiamen, China, pp. 558–560 (2012)

Publisher's Note

Mohammad Salah received his M.Sc. and Ph.D. degrees in Electrical Engineering from the Univresity of New Hampshire, NH, in 2003 and Clemson University, SC, in 2007, respectively. Upon receiving his B.Sc. degree in Engineering Technology in 2000, he worked as a control engieer at PALCO for Automation and Electrionic Control until 2002. In August 2007, he joined the Department of Mechatronics Enigineering at the Hashemite University, Jordan, where he is currently an associate professor. His research interests include applications of nonlinear control design in Mechatronics systems, MEMS, and automotive sysetms. E-mail: msalah@hu.edu.jo

Ahmad Al-Jarrah received his B.Sc. degree in Mechanical Engineering from Mutah University, Jordan in 1998. He completed his graduate studies towards the PhD in control systems from the University of Ottawa, Canada in 2007. Dr. Al-Jarrah joined the department of Mechatronics Engineering at the Hashemite University in 2008 as an assistant professor. He chaired the department for two years during which he got promoted to associate professor. Dr. Al-Jarrah has worked in a variety of areas and applications in mechatronics systems. His research of interest includes intelligent systems, linear and nonlinear control systems, automotive systems, control of MEMS, and robotics applications. E-mail: jarrah@hu.edu.jo

Enver Tatlicioglu received the B.Sc. degree in Electrical & Electronics Engineering from Dokuz Eylul University, Izmir, Turkey and the Ph.D. degree in Electrical and Computer Engineering from Clemson University, Clemson, SC, USA in 1999 and 2007, respectively. Upon completion of his Ph.D. degree, he worked as a post-doctoral research fellow in the Department of Electrical and Computer Engineering at Clemson University then he joined the Department of Electrical & Electronics Engineering at Izmir Institute of Technology, Izmir, Turkey where he is currently a full professor. His research interests include control and identification of time delay systems, dynamic modelling of extensible continuum robot manipulators, nonlinear control techniques for kinematically redundant robot manipulators, partial state feedback and output feedback control, haptic systems and teleoperation; learning, robust and adaptive control of non-linear systems. E-mail: envertatlicioglu@iyte.edu.tr.

Suleiman Bani Hani received the B.S. degree in mechanical engineering from Jordan University of Science and Technology in 2002, and the M.S. degree in mechanical engineering from Rensselaer Polytechnic Institute in 2004, and his Ph.D. degree in mechanical engineering from Rensselaer Polytechnic Institute in 2007. Dr. BaniHani is an Associate Professor at The Hashemite University. His research interests are artificial intelligence, computational mechanics, and control. E-mail: banihani@hu.edu.jo.